Journal of the Optical Society of America B
OPTICAL PHYSICS

Si-based near-infrared narrowband absorber based on square Au patches

XIAOYI LIU,[1,2] JINSONG GAO,[1,2] HAIGUI YANG,[2,*] AND XIAOYI WANG[2]

[1]University of the Chinese Academy of Sciences, Beijing 100039, China
[2]Key Laboratory of Optical System Advanced Manufacturing Technology, Changchun Institute of Optics, Fine Mechanics and Physics, Chinese Academy of Sciences, Changchun 130033, China
*Corresponding author: yanghg@ciomp.ac.cn

Received 11 July 2016; revised 30 August 2016; accepted 31 August 2016; posted 31 August 2016 (Doc. ID 270064); published 26 September 2016

We design a periodic Au patch-shaped microstructure covering on an Si substrate. This microstructure exhibits a designable near-infrared narrowband absorption from 1100 to 1500 nm. We investigate its absorption mechanism by the metal-insulator-metal waveguide theory and find that the combination of the plasmonic effect and cavity effect contributes an efficient absorption by calculating the electric field distribution numerically. We further analyze the relationship between the absorption spectra and electric field distributions of the structure with different patch lengths, by which we clarify why the narrowband absorption peak can be linearly shifted by varying the length of the Au patch.

OCIS codes: (040.6040) Silicon; (240.6680) Surface plasmons; (250.5403) Plasmonics.

http://dx.doi.org/10.1364/JOSAB.33.002149

1. INTRODUCTION

As an important component of nanophotonics, plasmonics has become a hot research topic in recent years. The interaction between electromagnetic radiation and conduction electrons at the interface of a metal/dielectric is the core content of plasmonics and usually needs a microstructure to help realize it [1–4]. To study the process of the interaction between substance and energy at the microscale would tend to produce some unexpected results. Most of plasmonics involve an optical near-field enhancement phenomenon on the subwavelength scale [5,6]. The essence of surface plasmon polaritons (SPPs) is a surface wave propagating along the interface of a metal/dielectric. Its penetration depth is limited by the kind of metal, the kind of dielectric, and the wavelength of the incident electromagnetic wave, and it is usually much smaller than the wavelength of incident light. Studies have shown that the penetration depth of the SPP on the metal side is only a few dozen nanometers, and it is produced by near-infrared light on a gold surface [7]. This means SPPs can confine the energy of incident electromagnetic waves to a thin range near the interface. This spatial compression of energy means plasmonics have a high potential value in many fields, such as solar cells [8,9], metamaterials [10,11], nonlinear optics [12,13], and surface-enhanced spectroscopy [14,15].

Another high-profile attraction of plasmonics is they can produce hot electrons efficiently through non-radiative decay [16,17]. These hot electrons can cross the Schottky barrier formed at a metal/semiconductor interface before thermalization and can be injected into the conduction band of a semiconductor, resulting in a photocurrent [7,16,17]. In other words, the conversion of the light signal into a photocurrent can be achieved by the plasmonic effect, which provides a very attractive pathway to realize a photodetector because its response range is not limited by the band gap of longer semiconductors. Accordingly, many research groups have proposed a variety of different metal/semiconductor microstructures to achieve a photoelectric response. Among them, the semiconductor Si is the most common substrate material [18,19]. As we all know, traditional Si-based devices are the most widely used because of their outstanding merits, such as their low cost, high performance, mature technology, and good compatibility. But they also have an obvious shortcoming, which is that they cannot absorb or respond to near-infrared light for wavelengths longer than 1200 nm owing to their large semiconductor band gap (1.12 eV) [20–22]. However, using plasmonics can effectively solve this problem. For an Si substrate covered with a metal microstructure, the factors limiting the photocurrent will no longer be its band gap, but the Schottky barrier at the interface of metal/Si. This offers the possibility to extend the response range of silicon-based detectors [19].

An unavoidable issue is that the absorption is the premise of efficient photoelectric conversion because it determines the upper limit of the photoelectric response. Therefore, prior to preparing the detector, exploring suitable microstructures on Si substrates to improve their absorptance is required. Here, we propose a periodic patch-shaped Au microstructure on

an Si substrate. We find that unlike other nanoarrays or nanoparticles [23–26], it can implement a designable narrowband absorption with an average absorptance around 75% in the near-infrared region from 1100 to 1500 nm by changing the Au microstructure size. A theoretical simulation indicates that the proposed microstructure not only generates a plasmonic effect, but it forms a cavity effect inside the grooves. Detailed discussions on the absorption mechanisms are given.

2. METHODOLOGY AND MODELING

Figure 1 shows the designed model of a periodic patch-shaped metal microstructure covering on an Si substrate. It consists of two-dimensional grating-shaped Au patches with a small air-space ratio, where we define the length (D) and the height (H) of the square Au patch to be the groove width (W) between two patches. In addition, we define the lateral angle (θ) of Au patch for the later discussion with an initial value of 90°. Considering the narrow grooves between neighboring patches, this nanoarray can also be treated as a structure containing metal-insulator-metal (MIM) waveguides [27], so we can do some mathematical descriptions with the MIM theory. First of all, we give the resonance condition in these waveguides [28],

$$2D\beta + \phi_r = 2m\pi, \tag{1}$$

where β is a complex propagation constant, and m is the resonance order. ϕ_r is the phase shift of propagating waves at two facets of the waveguide. According to this equation, we can figure out m just by using the value of β. Fortunately, complex propagation constant β can be obtained by solving the following dispersion equations [28]:

$$\begin{aligned} \epsilon_i k_m + \epsilon_m k_i \tanh(k_i W/2) &= 0 \\ \beta^2 - \epsilon_i k_0^2 &= k_i^2 \\ \beta^2 - \epsilon_m k_0^2 &= k_m^2, \end{aligned} \tag{2}$$

where ϵ_i and ϵ_m are the dielectric constants of the insulator and the metal, respectively. In this task, we have $\epsilon_i = 1$ and $\epsilon_m = \epsilon_{\mathrm{Au}}$. $k_0 = 2\pi/\lambda$ is the free space wave vector. Additionally, the effective refractive index n_e of the MIM waveguide can be defined as $n_e = \beta/k_0$. In summary, we can get the expression of resonance wavelength λ_r as follows:

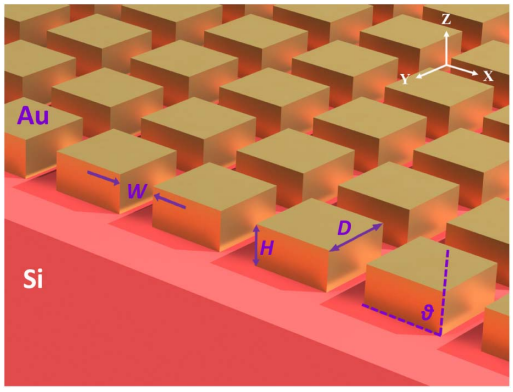

Fig. 1. Diagram of periodic patch-shaped Au microstructure on Si substrate.

$$\lambda_r = 2Dn_e/[m - (\phi_r/2\pi)]. \tag{3}$$

Substituting n_e and m into this expression will help us easily obtain λ_r. What is more, we can use it to provide a quantitative comparison and verification of the following simulations.

Subsequently, we use the finite-difference time-domain (FDTD) method to do simulations for the characteristics of the designed patch-shaped metal microstructures. Due to their symmetry, we adopted a non-polarized plane wave as the incidence source and set the periodic condition as the boundary condition in the X and Y directions. However, we used the perfectly matched layer (PML) condition in the Z direction in order to facilitate the measurement of the reflectance (R) and transmittance (T) and to calculate the absorptance (A) as $A = 1\text{-}R\text{-}T$. Meanwhile, we also adopted a high mesh accuracy (5 nm) to guarantee the simulation's convergence and verified its stability by a series of repeated simulations. All the aspects mentioned above should be paid attention to in modeling so we can ensure the reliability of the following calculations.

3. RESULTS AND DISCUSSION

First, we simulated the influence of D on the absorption. Figure 2(a) shows the near-infrared absorption curves with different D from 550 to 750 nm when $W = 50$ nm and $H = 200$ nm. All the absorption curves exhibit a narrowband characteristic, and the widths of half-maximum universally are about 100 nm, which is nearly three times smaller than the absorption spectrum widths in some works [16]. With the increase of D, the absorption peaks gradually shift to longer wavelengths. On the basis of Eq. (3), the peak wavelengths are assumed to be proportional to D, and we calculated the resonance wavelength λ_r by the MIM theory to contrast it with the results of the FDTD simulations. It should be noted that the phase-shift term $\phi_r/2\pi$ is included in the denominator of Eq. (3), resulting in a great influence on λ_r, so it cannot be treated as a constant for different D. Following the steps mentioned in Eqs. (1) and (2), we obtained the values of β and n_e with various systematic values of D, confirmed the resonance order ($m = 2$), and got the values of $\phi_r/2\pi$ when $D =$ 500 nm (0.5359) and $D = 750$ nm (0.2594) as well. Based

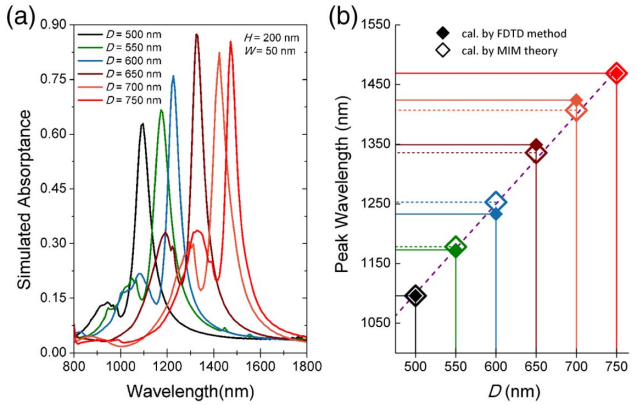

Fig. 2. (a) Dependence of simulated near-infrared light absorption on the length (D) of the square Au patch. (b) The relationship between D and the absorption peak wavelengths calculated by Eq. (3) and the FDTD simulations.

on them, we figured out the other phase-shift values by a linear fit, and then all the resonance wavelengths λ_r can be solved by substituting n_e with the phase-shift values we obtained. Figure 2(b) shows the relationship between D and the peak wavelengths we calculated by two methods. We can see that the results provided by Eq. (3) are in agreement with the results belong to the FDTD simulations, and the small deviations could be induced by the inappropriate fitting method for the phase shift. Clearly, the designed microstructure allows us to easily shift the position of the absorption peak by changing the structure size and therefore realize the designable narrowband absorption characteristics. Additionally, a very interesting phenomenon in Fig. 2(a) is that a secondary peak appears in the shorter wavelength region near each main peak in each absorption curve. Compared with the main peak, the secondary peak has slightly broader absorption band but much lower absorptance. Naturally, it can be regarded as the product of the higher-order resonance. In fact, it can be proven that there exists a fundamental resonance order in a longer wavelength band ($m = 1$). However, its absorption peak is relatively weak and outside of the scope of this paper, so we do not discuss it in detail.

Figure 3 shows the longitudinal electric field intensity distributions of the microstructure with $D = 550$ nm, $H = 200$ nm, and $W = 50$ nm when the incident light wavelengths are at 1067 and at 1173 nm, which precisely correspond to the positions of the secondary peak and the main peak in the absorption curve of Fig. 2(a). As shown in Fig. 3, the distribution details of the Au-Si interface indicate that SPPs excited by the periodic Au microstructure compress the energy in a very narrow range at the Au-Si interface and form electric field intensity arrangements alternately by a nodal distribution mode. Obviously, different distribution modes of the electric field intensity are formed by the SPP at the different wavelengths of 1173 and at 1067 nm. Here, we refer them to Mode 1 and Mode 2; these actually correspond to the second and third resonance orders. Mode 1 has a smaller number of anti-nodes but each anti-node is longer, while Mode 2 has a larger number of anti-nodes but they are shorter. It is a typical relationship between the alternate energy distribution and the waveguide mode or the resonance order [27]. Besides SPPs, the cavity effect [29–31] is also induced in the narrow grooves between neighboring Au patches. The cavity effect can tightly bound the energy of the incident light into the metal grooves

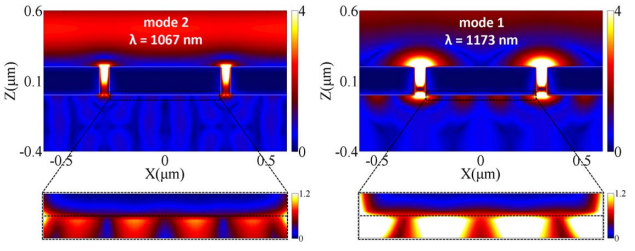

Fig. 3. Longitudinal (XY plane) electric field intensity distributions of the microstructure with $D = 550$ nm, $H = 200$ nm, and $W = 50$ nm when the incident light wavelengths are at 1173 and 1067 nm. The distribution details at the Au-Si interface are also given. The color bars stand for the normalized electric field intensity.

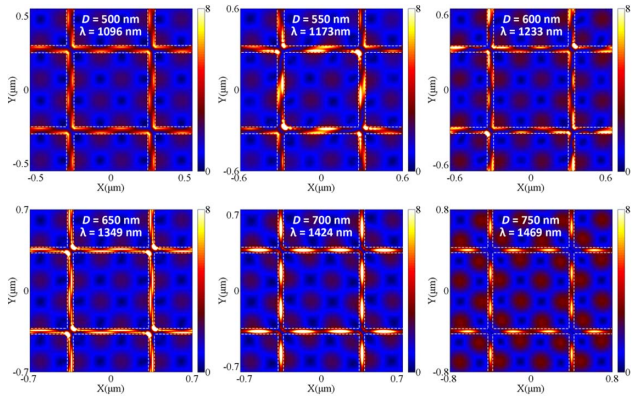

Fig. 4. Horizontal (XY plane) electric field intensity distributions of the microstructure at the Au-Si interface with different D at their main peak wavelengths, where $H = 200$ nm, $W = 50$ nm, and D ranges from 500–750 nm. The color bars stand for the normalized electric field intensity.

to realize a highly localized energy distribution and contribute to efficient absorption [19]. Clearly, from Fig. 3, it can be seen that the effect of the binding energy induced by the cavity effect at the wavelength of the main absorption peak is more dominant than that at the wavelength of the secondary absorption peak. It is confirmed that the cavity effect plays a positive role in the absorption of the microstructure.

For this patch-shaped metal microstructure, its electric field intensity distribution mode exists in more than the one-dimensional direction. Figure 4 shows the transverse electric field intensity distributions of the microstructure at the Au-Si interface with different D ranging from 500 to 750 nm, where $H = 200$ nm and $W = 50$ nm. The wavelengths of the incident light correspond to the main absorption peak positions of the microstructures. Obviously, the most significant point observed from Fig. 4 is that all the electric field intensities have almost the same distribution mode for the microstructures with different D, which means a similar mode of the standing wave is formed even though D changes. For a given mode, with an increase in D, the size of the anti-nodes also becomes large. Combined with Fig. 2, in other words, the absorption peak wavelength of the microstructure is proportional to the length of each anti-node as well. The deeper physical reason can be found in the resonance condition of Eq. (1), which provided further support for the inference indirectly mentioned in the preceding paragraphs.

In addition, we studied the influences of W and H of the Au patches on the near-infrared absorption of this microstructure [Figs. 5(a) and 5(b)]. It can be seen that the absorption peak wavelength is not sensitive to the changes of W and H, as expected by Eq. (3). Moreover, we introduced the concept of lateral angle θ, which is the angle between the sidewall of the Au patch and the Si substrate (see Fig. 1), and investigated its impact on the absorptance [Fig. 5(c)]. The absorption of the designed microstructure is sensitive to the lateral angle, as reflected in the decreasing absorption peak and the slightly shifting θ in the third diagram. In fact, Fig. 5(c) also implies that we should estimate deviations of the prepared samples in

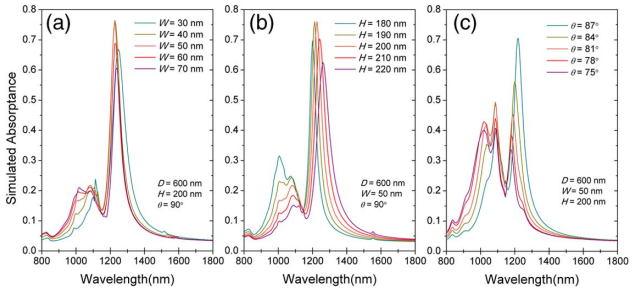

Fig. 5. (a) Absorption curves of the microstructure as a function of W when $D = 600$ nm, $H = 200$ nm, and $\theta = 90°$. (b) Absorption curves of the microstructure as a function of H when $D = 600$ nm, $W = 50$ nm, and $\theta = 90°$. (c) Absorption curves of the microstructure as a function of θ when $D = 600$ nm, $W = 50$ nm, and $H = 200$ nm.

advance, especially the lateral angle, because it is impossible to achieve the ideal perpendicularity in the fabrication process. Understanding this relationship between θ and the absorption will be helpful in evaluating the unavoidable imperfection, and in realizing this near-infrared narrowband-absorption microstructure experimentally.

Figure 6(a) shows a comparison between the absorption and the maximum electric field intensity of the microstructure with $D = 550$ nm, $H = 200$ nm, and $W = 50$ nm. Clearly, the trends of the two curves are nearly identical. At the absorption peak, its maximum electric field intensity is relatively stronger. It can be speculated that the electric field intensity determined its absorption spectrum, even the photoresponsivity. More concretely, the structure's photoresponsivity $R(\nu)$ can be expressed by the following equation [16,18]:

$$R(\nu) = A(\nu)\eta_1(\nu)\eta_2(\nu), \tag{4}$$

where $A(\nu)$ is the optical absorptivity, which is determined by the absorption spectrum and distributions. The absorption distributions can be calculated numerically by using the electric field distributions in Fig. 3 and the following expression of the local ohmic loss [18]:

$$Q(r,\omega) = \frac{1}{2}\omega\,\mathrm{Im}(\epsilon_m)|\vec{E}(r,\omega)|^2, \tag{5}$$

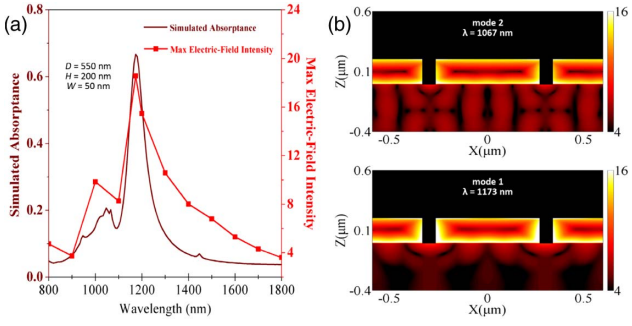

Fig. 6. (a) Comparison between the absorption and the maximum electric field intensity, and (b) the longitudinal (XY plane) absorption distributions of the microstructure with $D = 550$ nm, $H = 200$ nm, and $W = 50$ nm. The color bars stand for the calculated relative value of local ohmic loss (Q) in the logarithmic coordinate system.

where $\vec{E}(r,\omega)$ is the local electric field, and $\mathrm{Im}(\epsilon_m)$ is the imaginary part of the metal permittivity. From this expression, it can be said that the electric field distribution directly determines the level of absorption. Figure 6(b) shows the longitudinal absorption distributions of the same microstructure when the incident light wavelengths are at 1173 and at 1067 nm. Obviously, it has a strong absorption near Au surface, especially near the Au-Si interface. This absorption distribution is very helpful for the extraction of the photocurrent via hot electron generation when the designed microstructure is used as a photodetector [32]. It is mainly related to the concept of $\eta_1(\nu)$, which represents the probability of hot electrons arriving at the Schottky interface, and is determined by the generation locations of the hot electrons. Only when the motion tracks of the hot electrons fall within a specific cone determined by the distance from the Au-Si interface, the mean free path of the hot electrons and the Schottky barrier height [32], can they reach the Au-Si interface and cross the Schottky barrier to be injected into the conduction band of semiconductor, resulting in a photocurrent. In other words, the shorter the distance from the Au-Si interface, the greater the probability that hot electrons arrive at the Schottky interface. Therefore, from the photoelectric response point of view, the position near the Au-Si interface is the main area to produce effective hot electrons, and this absorption distribution is very advantageous to extract the photocurrent efficiently. As for the coefficient $\eta_2(\nu)$, it can be calculated by the following equation [16,18]:

$$\eta_2(\nu) = \mathrm{C_F}(h\nu - q\phi_B)/h\nu, \tag{6}$$

where $\mathrm{C_F}$ is the Fowler emission coefficient, $h\nu$ is the photon energy, and $q\phi_B$ is the Schottky barrier height between Si and Au. In general, on the basis of the discussion above, the designed structure can generate hot electrons primarily near the Schottky interface, which is the best way to increase the photoelectric conversion efficiency.

4. CONCLUSION

In summary, we have successfully demonstrated a near-infrared narrowband absorption by using a periodic patch-shaped Au microstructure covering on an Si substrate. A near-infrared absorption band with a width of about 100 nm and an average absorptance of 75% is designable from 1100 to 1500 nm for different lengths of Au patches. Its absorption peak wavelengths could be deduced by the MIM waveguide theory quantitatively, which agreed well with the results of the FDTD simulations. We confirmed that the energy was highly localized in the patch-shaped Au microstructure by the plasmonic and cavity effects, resulting in efficient absorption. Furthermore, we found that the electric fields near the Au-Si interface had almost the same distribution mode regardless of the length of Au patch, and each anti-node's length would change when length of the patch varied, which agreed with the mathematical analysis above. Accordingly, we can realize a linearly designable narrowband absorption by varying the length of the Au patch in a periodic patch-shaped Au microstructure covering on an Si substrate.

Funding. National Natural Science Foundation of China (NSFC) (U1435210, 61306125); Science and Technology

Innovation Project of Jilin Province (Y3293UM130, 20140101176JC); Science and Technology Innovation Foundation of CAS (CXJJ-15Q071); Science and Technology Innovation Project of CIOMP (Y3CX1SS143).

REFERENCES

1. M. R. Gadsdon, I. R. Hooper, A. P. Hibbins, and J. R. Sambles, "Surface plasmon polaritons on deep, narrow-ridged rectangular gratings," J. Opt. Soc. Am. B **26**, 1228–1237 (2009).
2. A. Dhibi, M. Khemiri, and M. Oumezzine, "Theoretical study of surface plasmons coupling in transition metallic alloy 2D binary grating," Physica E **79**, 160–166 (2016).
3. J. Yang, F. F. Luo, T. S. Kao, X. Li, G. W. Ho, J. H. Teng, X. G. Luo, and M. H. Hong, "Design and fabrication of broadband ultralow reflectivity black Si surfaces by laser micro/nanoprocessing," Light Sci. Appl. **3**, e185 (2014).
4. L. L. Huang, X. Z. Chen, B. F. Bai, Q. F. Tan, G. F. Jin, T. Zentgraf, and S. Zhang, "Helicity dependent directional surface plasmon polariton excitation using a metasurface with interfacial phase discontinuity," Light Sci. Appl. **2**, e70 (2013).
5. Q. Sun, K. Ueno, H. Yu, A. Kubo, Y. Matsuo, and H. Misawa, "Direct imaging of the near field and dynamics of surface plasmon resonance on gold nanostructures using photoemission electron microscopy," Light Sci. Appl. **2**, e118 (2013).
6. R. Ruppin, "Effect of non-locality on nanofocusing of surface plasmon field intensity in a conical tip," Phys. Lett. A **340**, 299–302 (2005).
7. R. Sundararaman, P. Narang, A. S. Jermyn, W. A. Goddard, and H. A. Atwater, "Design of plasmonic thin-film solar cells with broadband absorption enhancements," Nat. Commun. **5**, 5788 (2014).
8. R. A. Pala, J. White, E. Barnard, J. Liu, and M. L. Brongersma, "Design of plasmonic thin-film solar cells with broadband absorption enhancements," Adv. Mater. **21**, 3504–3509 (2009).
9. V. E. Ferry, L. A. Sweatlock, D. Pacifici, and H. A. Atwater, "Plasmonic nanostructure design for efficient light coupling into solar cells," Nano Lett. **8**, 4391–4397 (2008).
10. A. V. Kabashin, "Plasmonic nanorod metamaterials for biosensing," Nat. Mater. **8**, 867–871 (2009).
11. J. Henzie, M. H. Lee, and T. W. Odom, "Multiscale patterning of plasmonic metamaterials," Nat. Nano **2**, 549–554 (2007).
12. A. Popov, "Nonlinear optics of backward waves and extraordinary features of plasmonic nonlinear-optical microdevices," Eur. Phys. J. **58**, 263–274 (2010).
13. M. W. Klein, M. Wegener, N. Feth, and S. Linden, "Experiments on second- and third-harmonic generation from magnetic metamaterials," Opt. Express **15**, 5238–5247 (2007).
14. J. P. Camden, J. A. Dieringer, J. Zhao, and R. P. Van Duyne, "Controlled plasmonic nanostructures for surfaceenhanced spectroscopy and sensing," Acc. Chem. Res. **41**, 1653–1661 (2008).
15. E. J. R. Vesseur, R. De Waele, M. Kuttge, and A. Polman, "Direct observation of plasmonic modes in Au nanowires using high-resolution cathode luminescence spectroscopy," Nano Lett. **7**, 2843–2846 (2007).
16. M. W. Knight, H. Sobhani, P. Nordlander, and N. J. Halas, "Photodetection with active optical antennas," Science **332**, 702–704 (2011).
17. A. N. Mohammad, B. A. Fatih, B. T. Berk, and K. O. Ali, "Random sized plasmonic nanoantennas on silicon for low-cost broad-band near-infrared photodetection," Sci. Rep. **4**, 7103 (2014).
18. W. Li and J. Valentine, "Metamaterial perfect absorber based hot electron photodetection," Nano Lett. **14**, 3510–3514 (2014).
19. K. T. Lin, H. L. Chen, Y. S. Lai, and C. C. Yu, "Silicon-based broadband antenna for high responsivity and polarization-insensitive photodetection at telecommunication wavelengths," Nat. Commun. **5**, 3288 (2014).
20. Z. H. Huang, J. E. Carey, M. G. Liu, X. Y. Guo, E. Mazura, and J. C. Campbellb, "Microstructured silicon photodetector," Appl. Phys. Lett. **89**, 033506 (2006).
21. R. Younkin, J. E. Carey, E. Mazur, J. A. Levinson, and C. M. Friend, "Infrared absorption by conical silicon microstructures made in a variety of background gases using femtosecond-laser pulses," J. Appl. Phys. **93**, 2626–2629 (2003).
22. M. J. Smith, M. J. Sher, B. Franta, Y. T. Lin, E. Mazur, and S. Gradečak, "Improving dopant incorporation during femtosecond-laser doping of Si with a Se thin-film dopant precursor," Appl. Phys. A **114**, 1009–1016 (2014).
23. D. Chen, J. Zhou, M. Rippa, and L. Petti, "Structure-dependent localized surface plasmon resonance characteristics and surface enhanced Raman scattering performances of quasi-periodic nanoarrays: measurements and analysis," J. Appl. Phys. **118**, 163101 (2015).
24. A. Ravi, A. Luthra, F. L. Teixeira, P. R. Berger, and J. V. Coe, "Tuning the plasmonic extinction resonances of hexagonal arrays of Ag nanoparticles," Plasmonics **10**, 1505–1512 (2015).
25. C. Sun and X. Q. Wang, "Efficient light trapping structures of thin film silicon solar cells based on silver nanoparticle arrays," Plasmonics **10**, 1307–1314 (2015).
26. C. L. Haynes, A. D. McFarland, L. L. Zhao, R. P. V. Duyne, and G. C. Schatz, "Nanoparticle optics: the importance of radiative dipole coupling in two-dimensional nanoparticle arrays," J. Phys. Chem. B **107**, 7337–7342 (2003).
27. Y. Huang, X. Zhang, E. Ringe, M. J. Hou, L. W. Ma, and Z. J. Zhang, "Tunable lattice coupling of multipole plasmon modes and near-field enhancement in closely spaced gold nanorod arrays," Sci. Rep. **6**, 23159 (2016).
28. F. F. Hu, H. X. Yi, and Z. P. Zhou, "Band-pass plasmonic slot filter with band selection and spectrally splitting capabilities," Opt. Express **19**, 4848–4855 (2011).
29. Y. Zhu, X. Y. Hu, H. Yang, and Q. H. Gong, "On-chip plasmon-induced transparency based on plasmonic coupled nanocavities," Sci. Rep. **4**, 3752 (2014).
30. M. Qiao and R. Gordon, "Surface plasmon microcavity for resonant transmission through a slit in a gold film," Opt. Express **16**, 9708–9713 (2008).
31. K. Y. Wu, T. Rindzevicius, M. S. Schmidt, K. B. Mogensen, S. S. Xiao, and A. Boisen, "Plasmon resonances of Ag capped Si nanopillars fabricated using mask-less lithography," Opt. Express **23**, 12965–12978 (2015).
32. M. W. Knight, Y. M. Wang, A. S. Urban, A. Sobhani, B. Y. Zheng, P. Nordlander, and N. J. Halas, "Embedding plasmonic nanostructure diodes enhances hot electron emission," Nano Lett. **13**, 1687–1692 (2013).